A Sensor Array Realized by a Single Flexible TiO$_2$/POMs Film to Contactless Detection of Triacetone Triperoxide

Xiaorong Lü [1], Puqi Hao [1], Guanshun Xie [1], Junyuan Duan [2,*], Li Gao [1,*] and Bingxin Liu [1,*]

[1] Qinghai Provincial Key Laboratory of New Light Alloys, Qinghai Provincial Engineering Research Center of High Performance Light Metal Alloys and Forming, Qinghai University, Xining 810016, China; jwplxr@sina.com (X.L.); pheghost@outlook.com (P.H.); guanshunxie@126.com (G.X.)

[2] State Key Laboratory of Material Processing and Die & Mould Technology, School of Material Sciences and Engineering, Huazhong University of Science and Technology (HUST), Wuhan 430074, China

* Correspondence: junyuanduan@sina.com (J.D.); love_lier@163.com (L.G.); liubx408@nenu.edu.cn (B.L.); Tel.: +86-1869-723-5043 (B.L.)

check for updates

Abstract: The homemade explosive, triacetone triperoxide (TATP), is easy to synthesize, sensitive to detonation but hard to detect directly. Vapor sensor arrays composed of a few sensor materials have the potential to discriminate TATP, but the stability of the sensor array is always a tricky problem since each sensor may encounter a device fault. Thus, a sensor array based on a single optoelectronic TiO$_2$/PW$_{11}$ sensor was first constructed by regulating the excitation wavelength to discriminate TATP from other explosives. By in situ doping of Na$_3$PW$_{12}$O$_{40}$, a Keggin structure of PW$_{11}$ formed on the TiO$_2$ to promote the photoinduced electron-hole separation, thus obviously improving the detection sensitivity of the sensor film and shortening the response time. The response of the TiO$_2$/PW$_{11}$ sensor film to TATP under 365, 450 and 550 nm illumination is 81%, 42%, and 37%, respectively. The TiO$_2$/PW$_{11}$ sensor features selectivity to TATP and is able to detect less than 50 ppb. The flexibility and stability of the flexible sensor film is also demonstrated with the extent of bending. Furthermore, the sensing response cannot be affected by ambient air below 60% relative humidity.

Keywords: TATP; TiO$_2$; sensor array; POMs; gas sensitivity

1. Introduction

In recent years, explosive-based terrorism has grown extensively because explosive weapons have a simple manufacturing process, are easy to dispose of, and can cause enormous injury [1]. Peroxide-based explosives, such as triacetone triperoxide (TATP) [2], are the most powerful and dangerous and the first choice for terrorism all around the world. TATP has very high vapor pressure and is very sensitive to heat, impact, and explosion shock. Therefore, the development of sensor devices for explosive detection has great potential. As shown in Table S1, a few technologies, such as ion mobility spectrometry (IMS) [3,4], electrochemical method [5,6], colorimetric sensor [7,8] and gas sensing sensors [9–12], have been discovered in the field of trace TATP detection. IMS converts trace vapor into ions at atmospheric pressure and characterizes the gas phase mobility of these ions in a weak electric field to offer a highly efficient response to trace gas or vapor species. However, IMS equipment is expensive. The electrochemical method is always employed in a solution system. The colorimetric sensor possesses good accuracy but is very time consuming. Gas sensing sensors involve two key functions: (i) identification of a target gas via a gas–solid interaction, which causes an electron change of the oxide surface and (ii) conversion of the surface phenomena into resistance or current change of the sensor, called transducer function. Among them, the gas sensor is one of the most widely

used means in the market because of its advantages of quick response, high sensitivity, good stability, simple use, low cost, and so on.

In the field of sensors, TiO_2-semiconductor nanocrystals [13–18] become a flash point in the research of sensors owing to their large unique surface area, excellent optical response, excellent chemical stability, good biocompatibility and one-dimensional electron transport structure. However, the relatively wide band gap (3.2 eV) and low photoinduced charge carrier separation efficiency [19] hinder the practical application of TiO_2. To solve this problem, here we are proposing to develop a sensor based on polyoxometalates (POMs)-loaded TiO_2-semiconductor nanocrystal arrays.

POMs are composed of cations and polyanion clusters with structural diversity [20]. POMs are usually deemed to electron reservoirs because they have a strong ability to bear electrons and deliver electrons, illustrating their available redox nature [21]. So far, many classic paradigms of POMs, such as Keggin and Dawson structures, have been reported [22–25].

However, a single electrical sensor has difficulty in meeting the actual needs of qualitative identification of different explosives. In addition, the sensitivity and selectivity of single sensor are still a bottleneck for current solid sensors of gases. Naaman [26] developed an array of sensors based on non-specific interactions, which is capable of detecting TATP with high selectivity. Therefore, a sensor array is needed to make explosive identification possible. Nevertheless, the stability of the sensor array is always a tricky problem since each sensor may encounter a device fault. It would be very attractive if the function of a sensor array can be realized by only employing one sensor.

In this work, the regulating of the sensing properties of TiO_2 is achieved by the doping of POMs (sodium phosphotungstate, $Na_3O_{40}PW_{12}$), which dominates the surface states effectively in the Keggin structure to form $TiO_2/PW_{11}O_{39}$ (denoted as TiO_2/PW_{11} hereafter) and form a sensor array through the illumination of different wavelengths. We characterized the structure and morphology of the TiO_2/PW_{11} nanocrystals in detail and tested their properties, gaining insight into their sensitivity to the TATP explosive. In addition, we compared with pure TiO_2 and revealed the reason of the performance enhancement of the sensor doped with POMs.

2. Materials and Methods

2.1. Materials

Sodiumphosphotungstate ($Na_3O_{40}PW_{12}$), isopropyl alcohol (IPA), titanium tetraisopropoxide (TTIP) were of analytical grade. Standard distilled water was used in all experiments, sodium was an authenticated material purchased from the State Bureau of Technical Supervision, China.

2.2. Synthesis of TiO_2 and TiO_2/PW_{11} Nanocrystals

The pure TiO_2 was synthesized by 100 μL of titanium tetraisopropoxide (TTIP) diluted with 900 μL of isopropanol, and 708 μL of this solution was dripped with vigorous stirring into 29.3 mL distilled water at room temperature. After 20 h at 170 °C in a 40 mL Teflon-lined 316 stainless-steel reaction vessel, the solution was completely transparent and colorless. Then, the 30 mL solution was centrifuged using distilled water and dried at 60 °C to finally obtain pure TiO_2 powder.

The TiO_2/PW_{11} was synthesized as described by Weinstock [27]. A total of 100 μL of TTIP was diluted with 900 μL of isopropanol, and 708 μL of this solution dripped with vigorous stirring into 367 mg (0.12 mmol) of $Na_3O_{40}PW_{12}$ in 29.3 mL distilled water at room temperature. This gave 30 mL of a turbid (cream white) mixture, with a final concentration of 8 mM Ti (IV) and 4 mM $Na_3O_{40}PW_{12}$. After 20 h at 170 °C in a 40-mL Teflon-lined 316 stainless-steel reaction vessel, the solution was completely transparent and colorless with no precipitate. For isolation and purification of TiO_2/PW_{11} nanocrystals, the 30 mL solution was centrifuged using distilled water and NaCl because the primary POMs are fully soluble in NaCl solution. Four additional cycles of precipitation by adding NaCl, followed by centrifugation and redissolution in distilled water, eventually determined that trace amounts of POMs by-product were no longer present.

2.3. Characterization

Transmission electron microscopy (TEM) and Energy dispersive X-ray (EDS) mapping images was carried out on a JEM-2100F microscope. X-ray diffraction (XRD) patterns were measured using a Bruker D8 Advance X-ray diffractometer at a scanning rate of $6°$ min^{-1} with 2θ ranging from $20°$ to $80°$, using CuKα radiation ($\lambda = 1.5418$ Å). ^{31}P NMR spectra were recorded on a DRX-500 MHz (Bruker) spectrometer. FTIR spectra were recorded on a Magna 560 FT-IR spectrometer. UV/Vis absorption spectra were recorded on a Shimadzu UV-2550 UV/Vis spectrometer in the range 200–800 nm. An X-ray photoelectron spectroscopy (XPS, PHI5000 ESCA, Perkin Elmer, Waltham, MA, USA) equipped with an Al Kα source (1486.6 eV photons) was used to characterize the doping of POMs in TiO$_2$.

2.4. Device Fabrication and Gas Sensing Properties Testing

Interdigital gold electrodes are the hyperfine circuits obtained by electrochemical processing on polyimide (PI) substrate. The sensor film was constructed by dispersing TiO$_2$/PW$_{11}$ nanocrystals with different molar feed ratios into THF. Uniformly dripping onto the surface of the interdigital electrode, naturally drying, and repeating the above steps to obtain the TiO$_2$/PW$_{11}$ film. The thickness of the film was controlled by the dripping cycles. The sample was dried naturally in air overnight.

The different analytes were evaporated in a 50 mL transparent chamber and the test was conducted at room temperature in saturated 2,4,6-trinitrotoluene (TNT), 2,4-dinitrotoluene (DNT), picric acid (PA), hexogen (RDX), and 2,4,6-trinitrophenylmethylnitramine (Tetryl) vapor. Since TATP has very high vapor pressure at room temperature, it was diluted using air to 600 ppb. The time-dependent photoresponse of the sensor film was conducted in a conventional two electrode configuration and recorded by a Keithley 4200A-SCS Parameter Analyzer under 365, 450 and 550 nm monochromatic light. Thus, the sensor array based on the single optoelectronic TiO$_2$/PW$_{11}$ sensor was constructed by regulating the excitation wavelength (365, 450 and 550 nm).

3. Results and Discussion

3.1. Synthesis and Characterization of TiO$_2$/PW$_{11}$ Nanocrystals

TiO$_2$/PW$_{11}$ nanocrystals were obtained by hydrothermal reaction of titanium tetraisopropoxide, isopropanol and Na$_3$O$_{40}$PW$_{12}$ aqueous solution in distilled water for 20 h at 170 $°$C. TEM images of TiO$_2$/PW$_{11}$ nanocrystals (Figure 1a) show an average particle size of 5.9 $\pm$ 1.4 nm. Electron diffraction of the particles featured well-defined rings (Figure 1a inset), indicating that it is crystal structure. Of which, high-resolution TEM (HRTEM) images of the nanocrystals brings insight into the exposed (101) facets. Energy dispersive X-ray (EDS) mapping images (Figure 1c) display the presence and homogeneous distribution of titanium, tungsten and phosphorus elements in TiO$_2$/PW$_{11}$ samples. These results confirm the formation of TiO$_2$/PW$_{11}$ composite.

To consider the crystalline phases and the crystallinity of the TiO$_2$/PW$_{11}$ nanocrystals, X-ray diffraction (XRD) characterization was conducted (Figure 2). It is worth mentioning that the crystalline structure of the TiO$_2$/PW$_{11}$ remained in anatase phases TiO$_2$ since diffraction peaks are observed at $25.3°$, $37.8°$, $48.0°$, $55.1°$, and $62.7°$ [28,29]. However, the diffractions originated from the interaction between POMs and TiO$_2$ are hard to observe; this might be attribute to the interaction of phosphotungstate in the octahedral interstitial site or the substitutional position of TiO$_2$. These results indicated the phosphotungstate might interact with titania through oxygen atoms and that one W atom in Na$_3$O$_{40}$PW$_{12}$ was substituted to form the Keggin structure of TiO$_2$/PW$_{11}$ [30]. Moreover, Debye–Scherrer analysis of XRD data gave an anatase–crystallite size of 4.89 $\pm$ 0.2 nm, basically identical to the average particle size obtained from TEM images.
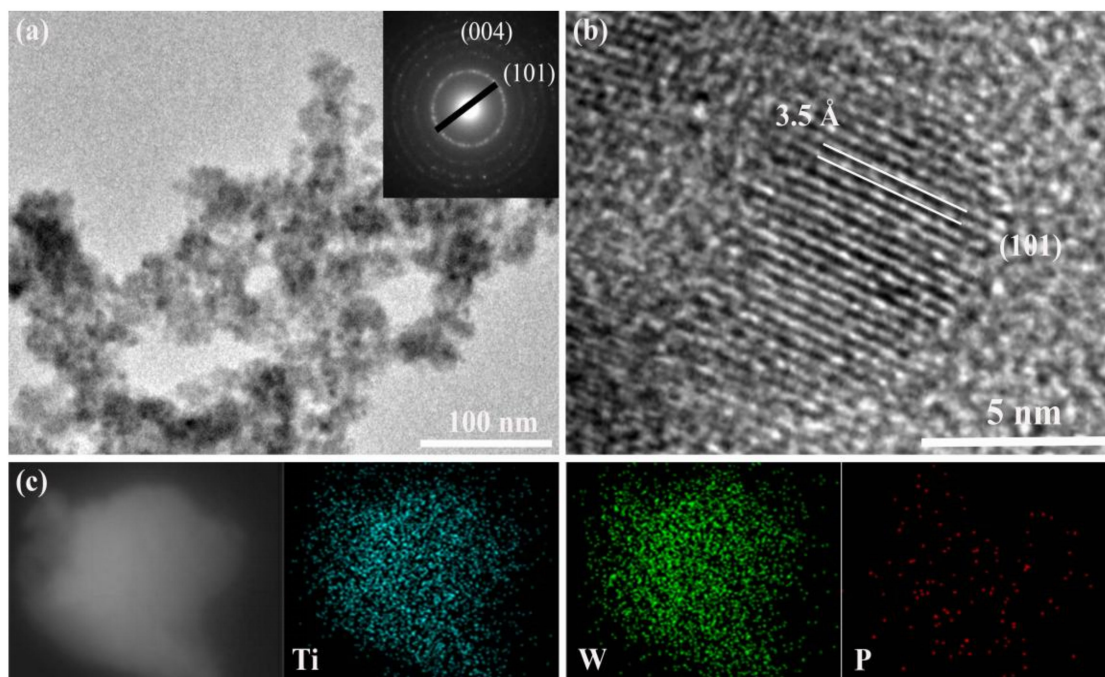
Figure 1. Characterization of TiO$_2$/PW$_{11}$ nanocrystals. (**a**) TEM image of TiO$_2$/PW$_{11}$ nanocrystals; inset: selected-area electron diffraction pattern of the particles. (**b**) HRTEM image of TiO$_2$/ PW$_{11}$ nanocrystals with fringes corresponding to (101) planes. (**c**) EDS elemental mapping images of Ti, W and P.
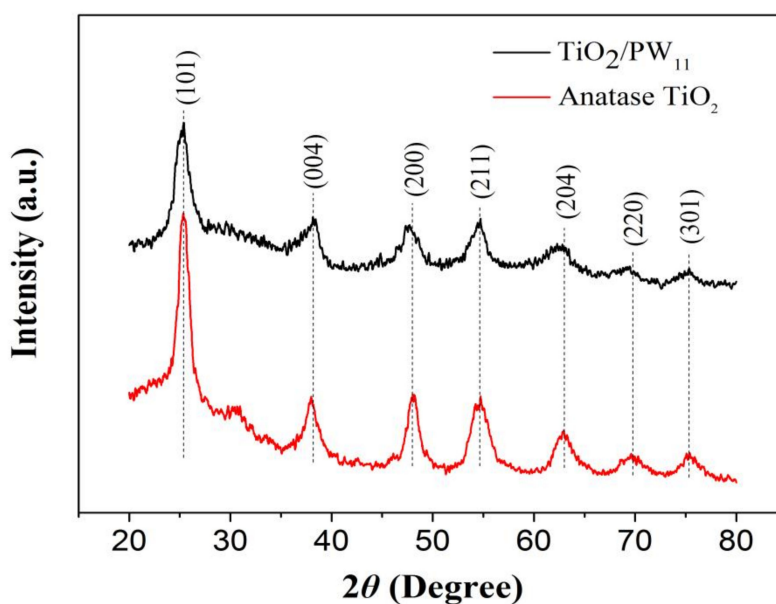

Figure 2. XRD patterns of the anatase TiO$_2$ and TiO$_2$/PW$_{11}$.

The Keggin type structure of PW$_{11}$ formed in TiO$_2$ nanocrystals was further proved by FTIR (Figure 3). The characteristic bands observed at 1089, 1066, and 953 cm^{-1} in TiO$_2$/PW$_{11}$ nanocrystal attributes to vibrations of P-O, W-O-W and W-O [29], which are not found in TiO$_2$/PW$_{11}$ nanocrystals. These results prove the Keggin PW$_{11}$ has been successfully modified on TiO$_2$.

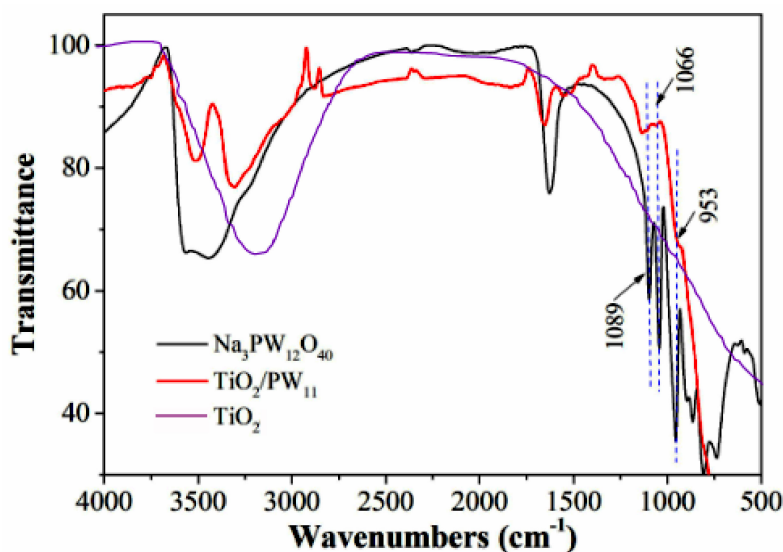**Figure 3.** FTIR spectra of $Na_3PW_{12}O_{40}$, TiO_2/PW_{11} and TiO_2.

Solid-state ^{31}P CPMAS NMR spectroscopy of TiO_2/PW_{11} nanocrystals showed a single broad signal Keggin unit at $\delta = -13.9$ ppm (Figure 4). Thus showing the formation of a single phosphorus-containing species and that the molecular structure in the solid state was retained in the sample [28].
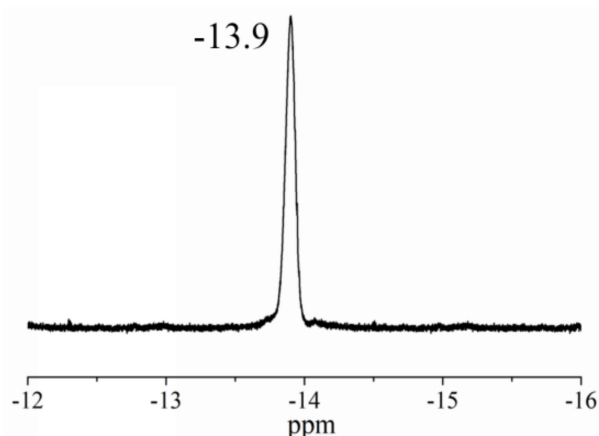

Figure 4. Solid-state ^{31}P NMR spectra of TiO_2/PW_{11} nanocrystals.

The POMs deposited onto a TiO_2 were also analyzed by X-ray photoelectron spectroscopy (XPS). As shown in Figure 5, the binding energy (BE) of Ti $2p_{2/1}$ and Ti $2p_{3/2}$ from Ti^{4+} can be detected at 458.54 eV and 464.39 eV [31]. The XPS spectra of W $4f_{5/2}$ and W $4f_{7/2}$ show the BE at 35.38 and 37.49 eV [31]. This is further proof for the adsorption of PW_{11} onto the TiO_2. Moreover, the XPS measurements were performed to reveal the atomic content (Table S2). Based on the peak areas of W and Ti, it can be concluded that approximately 3.94% of the W is on the surface of the TiO_2 (the content of TiO_2 is 17.6%).
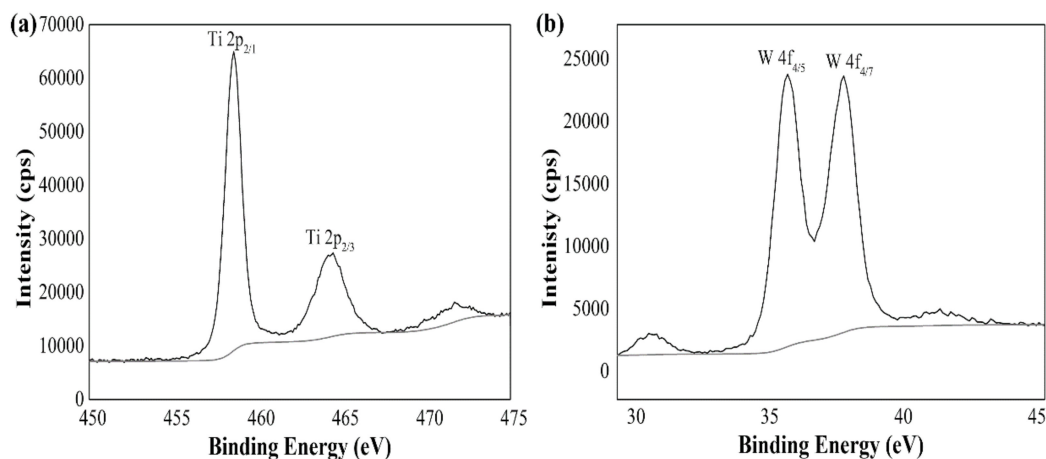
Figure 5. XPS spectra of Ti (**a**) and W (**b**).

3.2. Optoelectronic Gas Sensor Properties

The sensing properties of the TiO_2/PW_{11} sensor film (Figure 6a) to different explosives vapor (TATP, TNT, DNT, RDX, PA and tetryl, respectively) were evaluated under different illumination wavelengths (Figure 6c: 365 nm, Figure 6d: 450 nm, and Figure 6e: 550 nm). The TiO_2/PW_{11} sensor film was coated onto the interdigital gold electrodes. The electrodes were obtained by electrochemical processing on a flexible PI substrate, and, as shown in Figure 6b, the line width and spacing were 95 µm and 115 µm. Response values of TiO_2/PW_{11} sensor film to different explosives vapor under different illumination wavelengths are summarized in Table 1. One can see from Figure 6 that, for example, the response (defined as $(I_t - I_0)/I_0$) of TiO_2/PW_{11} sensor film to TATP under 365, 450 and 550 nm illumination was 84%, 42%, and 37%, respectively. It is obvious that the responses of TiO_2/PW_{11} sensor film toward TATP were larger than those of other explosives under different illumination wavelengths. What is in strong contrast is that, as shown in Figure S1, the responses of pure TiO_2 toward various explosives were all below 1% under 365 nm illumination. No obvious response could be detected for pure TiO_2 toward all tested explosives under the illuminations of 450 nm and 550 nm. This result reveals that POMs played a vital role to deliver photogenerated electrons in TiO_2. The excellent response of TiO_2/PW_{11} sensor film to TATP may be roughly attributed to the absorption of TATP on the surface of TiO_2/PW_{11}, coupled with photocatalytic decomposition of TATP to acetone and H_2O_2. Under the irradiation of light, the photoelectron in conduction band (CB) of TiO_2 transfers to HOMO of POMs. Thus, the photocurrent from the TiO_2/PW_{11} system promoted the photocatalytic activity of sensor film. Consequently, the sensor film had better performance when it was under the conditions of ultraviolet and visible light.

Additionally, as depicted in Figure 6f–h, the response times of TATP were 4, 7, and 5 s while the decay times of TATP were 5, 10, and 5 s, respectively. The response time and decay time of other explosives were all within 10 s. This fast reaction process originates from the ability of POMs to deliver electrons. To demonstrate the role of POMs doped in TiO_2, the UV-visible spectra of $Na_3PW_{12}O_{40}$, anatase TiO_2 and TiO_2/PW_{11} was presented in Figure 7. Compared with the UV absorption at 305 nm of anatase TiO_2, the absorption of TiO_2/PW_{11} at 305 nm was dismissed, which may originate from the strong ability of POMs to bear electrons and deliver photoelectrons of TiO_2, and thus the photoinduced charge carrier's separation efficiency was improved [32,33].
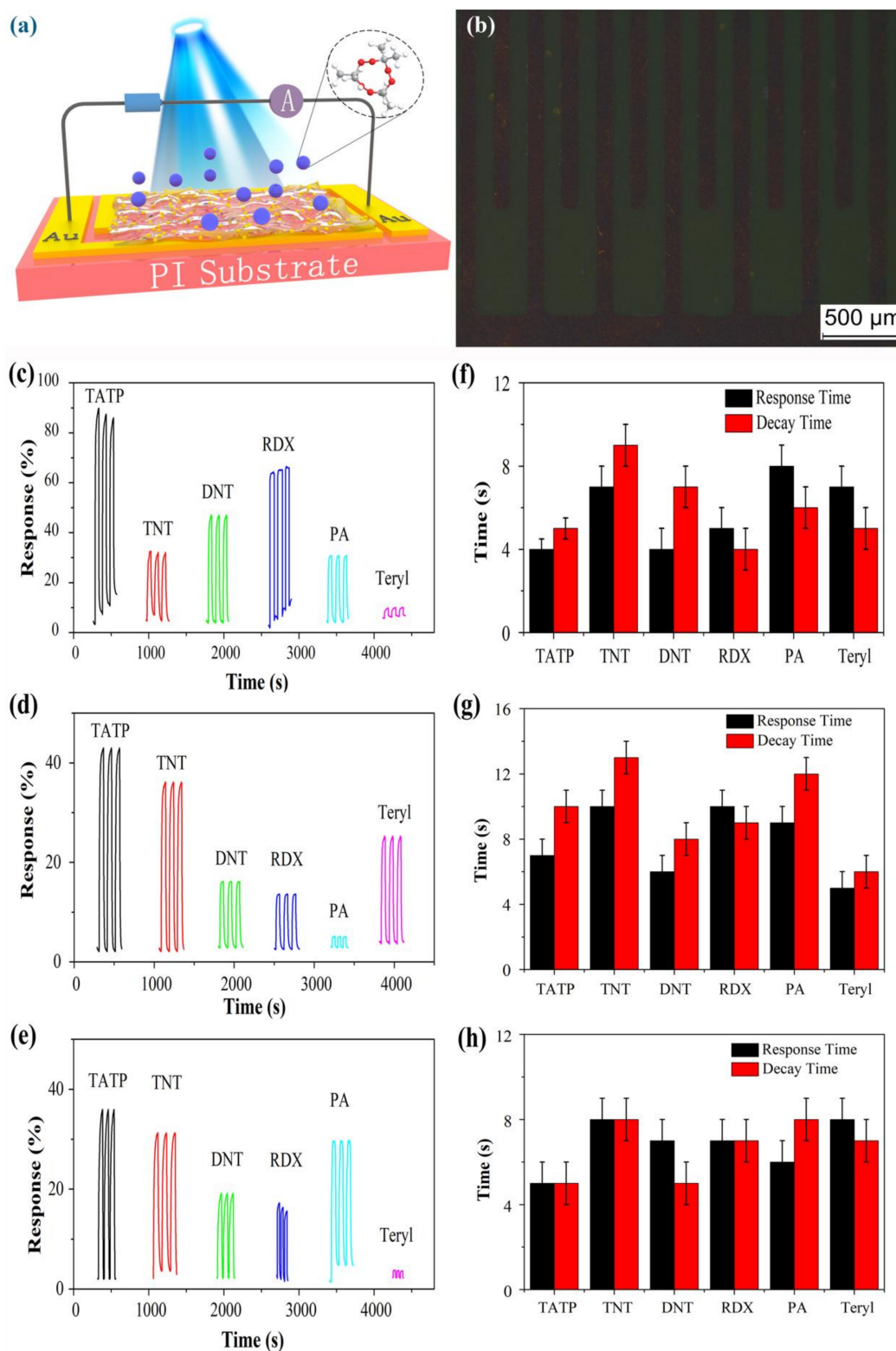
Figure 6. (**a**) Schematic diagram of a sensor film constructed from TiO_2/PW_{11} nanocrystals. (**b**) Microstructure of interdigital gold electrodes on PI substrate. Response of TiO_2/PW_{11} to different explosives under (**c**) 365 nm, (**d**) 450 nm and (**e**) 550 nm illumination. Response time and decay time of TiO_2/PW_{11} sensor film under (**f**) 365 nm, (**g**) 450 nm and (**h**) 550 nm illumination.

Table 1. Response value of TiO_2/PW_{11} sensor film to different explosives vapor under different illumination wavelengths.

Illumination Wavelengths	365 nm			450 nm			550 nm		
Response Value	R [1] (%)	R T [2] (s)	D T [3] (s)	R (%)	R T (s)	D T (s)	R (%)	R T (s)	D T (s)
TATP	81	4	5	42	7	10	37	5	5
TNT	37	7	9	37	10	13	32	8	8
DNT	45	4	7	18	5	8	19	7	5
RDX	69	5	4	14	10	9	17	7	7
PA	32	8	6	4	9	12	30	6	8
Tetryl	8	7	5	28	4	6	2	8	6

[1] Response (defined as $(I_t - I_0)/I_0$). [2] Response time. [3] Decay time.
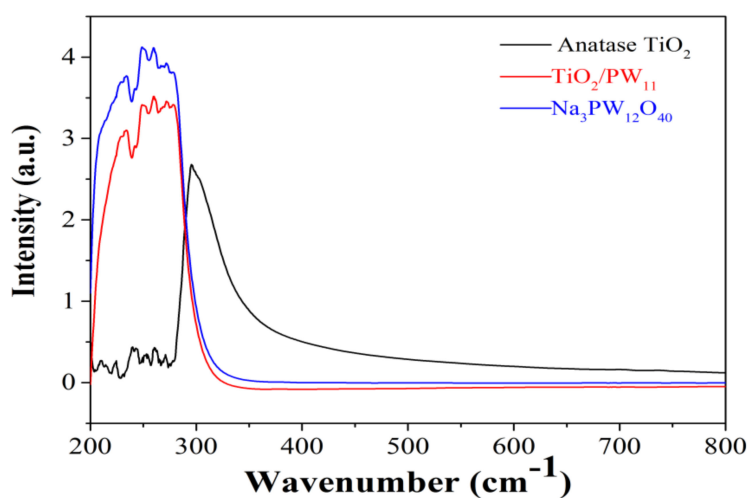
Figure 7. UV-visible spectrum of $Na_3PW_{12}O_{40}$ (blue line), anatase TiO_2 (black line) and TiO_2/PW_{11} (red line).

Figure 8a presents the response of the TiO_2/PW_{11} when introduced to vapors of TATP at variable concentrations under 365 nm illumination. TATP was diluted using nitrogen from 550 ppb to 50 ppb. It was difficult to obtain concentrations below 50 ppm with high enough accuracy under our current experimental conditions and therefore the lowest concentration measured was 50 ppb of TATP. The TiO_2/PW_{11} showed an obvious response of about 20% when the TATP concentration was lowered to 50 ppm, which is lower than that of hybrid organic-semiconductor sensors [26]. Figure 8b shows the liner response of TiO_2/PW_{11} to TATP vapor at concentrations from 450 to 50 ppm. In addition, the response of the sensor decreased in the range of 57.67%–19.75%.

Generally, optoelectronic sensing shows great advantages for the high sensitivity in the field of gas sensing. However, a single sensor film can respond to different explosives vapor but cannot discriminate them from each other. The sensor array was constructed using various materials to discriminate target molecules using the statistical procedure in previous work [26]. Here, a sensor array based on the above single optoelectronic TiO_2/PW_{11} sensor was constructed by regulating the excitation wavelength. Principal component analysis (PCA) was employed to evaluate the recognition capability of the sensor array. This process has been described by Brady, where MATLAB was used to perform the PCA and classification [34]. As shown in Table 1, 54 characteristic response parameters (response, response time and decay time under 365, 450 and 550 nm illumination) were integrated for all the data. A training set of three runs for each explosive (18 runs total; 18 × 54 matrix) was subjected to PCA, yielding a 54 × 54 matrix containing the eigenvectors for the data set. Figure 9 shows the projection of the training data using three of the six principal components for the six explosives.

The results obtained from the PCA showed that the cluster of six different explosives congregated separately and independent of each other, allowing for accurate classification. Therefore, the sensor array based on a single TiO$_2$/PW$_{11}$ can well distinguish TATP from six different explosives.
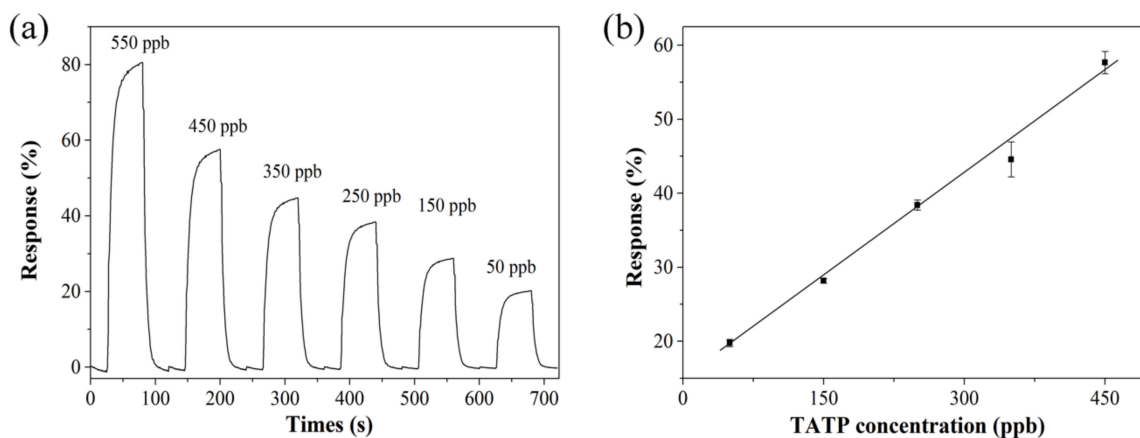

Figure 8. (**a**) The response measured for the TiO$_2$/PW$_{11}$ exposed to decreasing concentrations of TATP under 365 nm illumination. (**b**) The calibration curve based on the data from (**a**), the slope of the plot is 0.09 and R-square = 0.99.
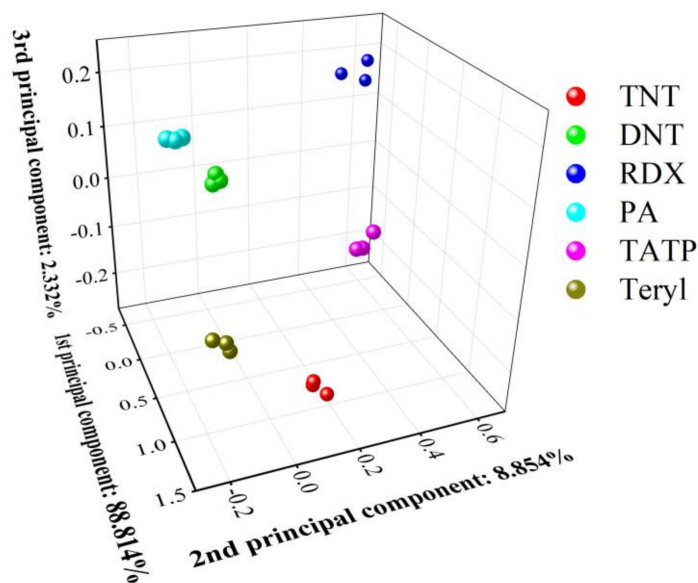

Figure 9. The principal component analysis (PCA) plot of the response values.

Furthermore, the flexibility and stability of the flexible sensor film was demonstrated with the bending test. As shown in Figure 10a–c, no significant decrease in the response of sensor film of TATP was found compared to the relaxed state, down to a curvature of 15 mm under the illumination of 365 nm, 450 nm and 550 nm. Repetitive bending (for 50 cycles) did not degrade the sensor performance, which suggests good flexibility and mechanical endurance of the sensor film.

Metal oxide semiconductor nanomaterial is always sensitive to humidity. Many works have developed various methods to minimize the effect of humidity on explosive sensing [35]. Here, the role of relative humidity (RH) is addressed in Figure 10d–f. The response ratios of TATP are almost unchanged, at 20%, 40% and 60% RH under the illumination of 365 nm, 450 nm and 550 nm. However, the response ratio of TATP decreased at 80% RH due to competitive adsorption of TATP and water molecules on the surface of TiO$_2$/PW$_{11}$ film. This result illustrates that the sensing response cannot be affected by ambient air below the 60% RH.

The long-term stability of the flexible sensor film was also studied (Figure S2). The TiO_2/PW_{11} film has high stability and did not degrade the response to TATP for at least five months under the illumination of 365 nm, 450 nm and 550 nm. Thus, the TiO_2/PW_{11} sensor film showed excellent long-term stability to TATP, which shows potential for practical usage.

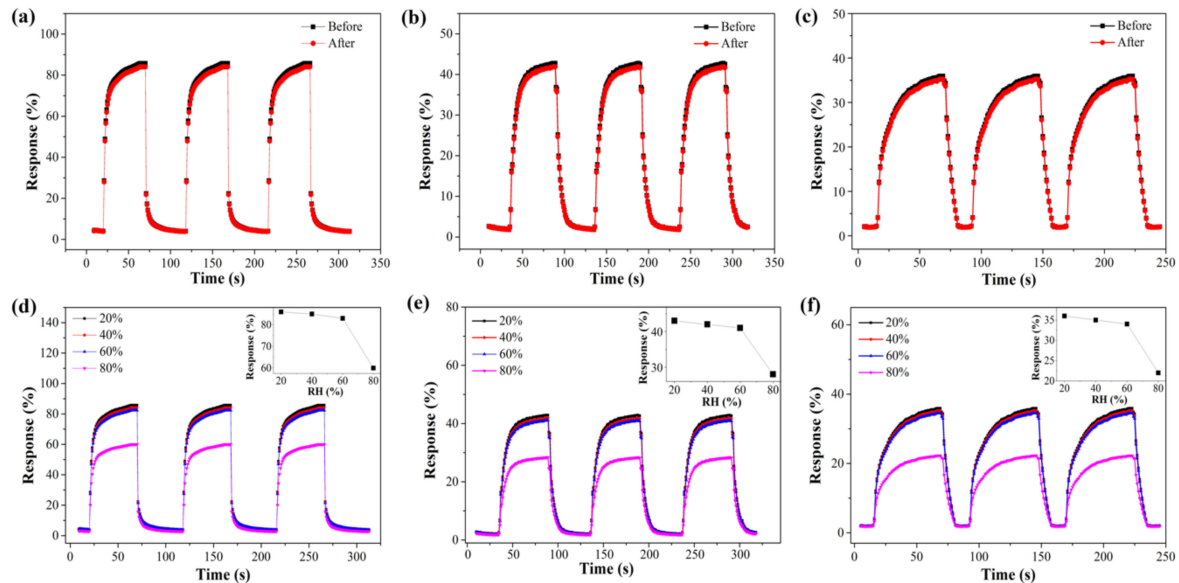**Figure 10.** The response of the sensor film to TATP before and after bending under the illumination of 365 nm (**a**), 450 nm (**b**) and 550 nm (**c**). Effect of the humidity under the illumination of 365 nm (**d**), 450 nm (**e**) and 550 nm (**f**).

4. Conclusions

Keggin structure PW_{11} doped TiO_2/PW_{11} was constructed by in situ doping of $Na_3PW_{12}O_{40}$ into $TiO_{\neg2}$. The function of a sensor array toward an improvised explosive, TATP, can be realized by employing only a TiO_2/PW_{11} sensor by adjusting the illumination wavelength. The TATP vapor sensing property of the sensor film significantly depended on the illumination wavelength. The remarkable improvement in gas sensing performance under light illumination was attributed to the Keggin POM structures on the surface of $TiO_{\neg2}$ because the POMs have a strong ability to bear and deliver electrons. Thus, the number of electrons that participate in the reaction with TATP gas molecules greatly increases. We expect that this study will shine light on the realization of portable, real-time, and cheap platforms for contactless discrimination of explosive monitoring.

References

1. Wu, Z.; Zhou, C.; Zu, B.; Li, Y.; Dou, X. Contactless and Rapid Discrimination of Improvised Explosives Realized by Mn^{2+} Doping Tailored ZnS Nanocrystals. *Adv. Funct. Mater.* **2016**, *26*, 4578–4586. [CrossRef]

2. Ray, R.S.; Sarma, B.; Mohanty, S.; Misra, M. Theoretical and experimental study of sensing triacetone triperoxide (TATP) explosive through nanostructured TiO_2 substrate. *Talanta* **2014**, *118*, 304–311. [CrossRef] [PubMed]

3. Nagarkar, S.S.; Joarder, B.; Chaudhari, A.K.; Mukherjee, S.; Ghosh, S.K. Highly Selective Detection of Nitro Explosives by a Luminescent Metal–Organic Framework. *Angew. Chem. Int. Ed.* **2013**, *52*, 2881–2885. [CrossRef] [PubMed]

4. Peng, L.; Hua, L.; Wang, W.; Zhou, Q.; Li, H. On-site Rapid Detection of Trace Non-volatile Inorganic Explosives by Stand-alone Ion Mobility Spectrometry via Acid-enhanced Evaporization. *Sci. Rep.* **2014**, *4*, 6631. [CrossRef] [PubMed]

5. Mamo, S.K.; Gonzalez-Rodriguez, J. Development of a Molecularly Imprinted Polymer-Based Sensor for the Electrochemical Determination of Triacetone Triperoxide (TATP). *Sensors* **2014**, *14*, 23269–23282. [CrossRef] [PubMed]

6. Laine, D.F.; Roske, C.W.; Cheng, I.F. Electrochemical detection of triacetone triperoxide employing the electrocatalytic reaction of iron(II/III)-ethylenediaminetetraacetate and hydrogen peroxide. *Anal. Chim. Acta* **2008**, *608*, 56–60. [CrossRef] [PubMed]

7. Can, Z.; Üzer, A.; Türkekul, K.; Erçağ, E.; Apak, R. Determination of Triacetone Triperoxide with a *N,N*-Dimethyl-p-phenylenediamine Sensor on Nafion Using Fe_3O_4 Magnetic Nanoparticles. *Anal. Chem.* **2015**, *87*, 9589–9594. [CrossRef] [PubMed]

8. Üzer, A.; Durmazel, S.; Erçağ, E.; Apak, R. Determination of hydrogen peroxide and triacetone triperoxide (TATP) with a silver nanoparticles-based turn-on colorimetric sensor. *Sens. Actuators B Chem.* **2017**, *247*, 98–107. [CrossRef]

9. Warmer, J.; Wagner, P.; Schöning, M.J.; Kaul, P. Detection of triacetone triperoxide using temperature cycled metal-oxide semiconductor gas sensors. *Phys. Status Solidi* **2015**, *212*, 1289–1298. [CrossRef]

10. Yang, Z.; Dou, X.; Zhang, S.; Guo, L.; Zu, B.; Wu, Z.; Zeng, H. A High-Performance Nitro-Explosives Schottky Sensor Boosted by Interface Modulation. *Adv. Funct. Mater.* **2015**, *25*, 4039–4048. [CrossRef]

11. Schnorr, J.M.; van der Zwaag, D.; Walish, J.J.; Weizmann, Y.; Swager, T.M. Sensory Arrays of Covalently Functionalized Single-Walled Carbon Nanotubes for Explosive Detection. *Adv. Funct. Mater.* **2013**, *23*, 5285–5291. [CrossRef]

12. Han, C.-H.; Hong, D.-W.; Han, S.-D.; Gwak, J.; Singh, K.C. Catalytic combustion type hydrogen gas sensor using TiO_2 and UV-LED. *Sens. Actuators B Chem.* **2007**, *125*, 224–228. [CrossRef]

13. Mor, G.K.; Varghese, O.K.; Paulose, M.; Shankar, K.; Grimes, C.A. A review on highly ordered, vertically oriented TiO_2 nanotube arrays: Fabrication, material properties, and solar energy applications. *Sol. Energy Mater. Sol. Cells* **2006**, *90*, 2011–2075. [CrossRef]

14. Ozawa, K.; Yamamoto, S.; Yukawa, R.; Liu, R.-Y.; Terashima, N.; Natsui, Y.; Kato, H.; Mase, K.; Matsuda, I. Correlation between Photocatalytic Activity and Carrier Lifetime: Acetic Acid on Single-Crystal Surfaces of Anatase and Rutile TiO_2. *J. Phys. Chem. C* **2018**, *122*, 9562–9569. [CrossRef]

15. Banerjee, S.; Mohapatra, S.K.; Das, P.P.; Misra, M. Synthesis of Coupled Semiconductor by Filling 1D TiO_2 Nanotubes with CdS. *Chem. Mater.* **2008**, *20*, 6784–6791. [CrossRef]

16. Mohapatra, S.K.; Misra, M.; Mahajan, V.K.; Raja, K.S. Design of a Highly Efficient Photoelectrolytic Cell for Hydrogen Generation by Water Splitting: Application of $TiO_{2-x}C_x$ Nanotubes as a Photoanode and Pt/TiO_2 Nanotubes as a Cathode. *J. Phys. Chem. C* **2007**, *111*, 8677–8685. [CrossRef]

17. Banerjee, S.; Mohapatra, S.K.; Misra, M.; Mishra, I.B. The detection of improvised nonmilitary peroxide based explosives using a titania nanotube array sensor. *Nanotechnology* **2009**, *20*, 75502. [CrossRef] [PubMed]

18. Wang, W.; Song, H.; Liu, Q.; Bai, X.; Wang, Y.; Dong, B. Modified optical properties in a samarium doped titania inverse opal. *Opt. Lett.* **2010**, *35*, 1449–1451. [CrossRef]

19. Yan, X.; Xu, Y.; Tian, B.; Lei, J.; Zhang, J.; Wang, L. Operando SERS self-monitoring photocatalytic oxidation of aminophenol on TiO_2 semiconductor. *Appl. Catal. B Environ.* **2018**, *224*, 305–309. [CrossRef]

20. Sharma, M.; Saikia, G.; Ahmed, K.; Gogoi, S.R.; Puranik, V.G.; Islam, N.S. Vanadium-based polyoxometalate complex as a new and efficient catalyst for phenol hydroxylation under mild conditions. *New J. Chem.* **2018**, *42*, 5142–5152. [CrossRef]

21. Zhang, X.-X.; Yuan, H.; Yu, W.-D.; Gu, Y.-Y.; Yan, J. Synthesis and characterization of two benzylarsonate functionalized polyoxomolybdates with catalytic activity for oxidation of benzyl alcohol to benzaldehyde. *Inorg. Chem. Commun.* **2018**, *91*, 77–80. [CrossRef]

22. Makrygenni, O.; Secret, E.; Michel, A.; Brouri, D.; Dupuis, V.; Proust, A.; Siaugue, J.-M.; Villanneau, R. Heteropolytungstate-decorated core-shell magnetic nanoparticles: A covalent strategy for polyoxometalate-based hybrid nanomaterials. *J. Colloid Interface Sci.* **2018**, *514*, 49–58. [CrossRef] [PubMed]

23. Ma, Y.; Peng, H.; Liu, J.; Wang, Y.; Hao, X.; Feng, X.; Khan, S.U.; Tan, H.; Li, Y. Polyoxometalate-Based Metal–Organic Frameworks for Selective Oxidation of Aryl Alkenes to Aldehydes. *Inorg. Chem.* **2018**, *57*, 4109–4116. [CrossRef] [PubMed]

24. Sun, K.; Li, H.; Ye, H.; Jiang, F.; Zhu, H.; Yin, J. 3D-Structured Polyoxometalate Microcrystals with Enhanced Rate Capability and Cycle Stability for Lithium-Ion Storage. *ACS Appl. Mater. Interfaces* **2018**, *10*, 18657–18664. [CrossRef] [PubMed]

25. Nohra, B.; El Moll, H.; Rodriguez Albelo, L.M.; Mialane, P.; Marrot, J.; Mellot-Draznieks, C.; O'Keeffe, M.; Ngo Biboum, R.; Lemaire, J.; Keita, B.; et al. Polyoxometalate-Based Metal Organic Frameworks (POMOFs): Structural Trends, Energetics, and High Electrocatalytic Efficiency for Hydrogen Evolution Reaction. *J. Am. Chem. Soc.* **2011**, *133*, 13363–13374. [CrossRef] [PubMed]

26. Capua, E.; Cao, R.; Sukenik, C.N.; Naaman, R. Detection of triacetone triperoxide (TATP) with an array of sensors based on non-specific interactions. *Sens. Actuators B Chem.* **2009**, *140*, 122–127. [CrossRef]

27. Raula, M.; Gan Or, G.; Saganovich, M.; Zeiri, O.; Wang, Y.; Chierotti, M.R.; Gobetto, R.; Weinstock, I.A. Polyoxometalate Complexes of Anatase-Titanium Dioxide Cores in Water. *Angew. Chem.* **2015**, *127*, 12593–12598. [CrossRef]

28. Yusuke, M.; Yuki, M.; Yoshitaka, S.; Satoshi, M.; Kenji, N. Monomer and Dimer of Mono-titanium(IV)-Containing α-Keggin Polyoxometalates: Synthesis, Molecular Structures, and pH-Dependent Monomer–Dimer Interconversion in Solution. *Eur. J. Inorg. Chem.* **2013**, *2013*, 1754–1761.

29. Vorontsov, A.V.; Tsybulya, S.V. Influence of Nanoparticles Size on XRD Patterns for Small Monodisperse Nanoparticles of Cu^0 and TiO_2 Anatase. *Ind. Eng. Chem. Res.* **2018**, *57*, 2526–2536. [CrossRef]

30. Lu, N.; Zhao, Y.; Liu, H.; Guo, Y.; Yuan, X.; Xu, H.; Peng, H.; Qin, H. Design of polyoxometallate–titania composite film ($H_3PW_{12}O_{40}/TiO_2$) for the degradation of an aqueous dye Rhodamine B under the simulated sunlight irradiation. *J. Hazard. Mater.* **2012**, *199–200*, 1–8. [CrossRef] [PubMed]

31. Ji, Y.; Li, T.; Song, Y.-F. Adsorption of Human Serum Albumin (HSA) by SWNTs/Py-PW_{11} Nanocomposite. *Ind. Eng. Chem. Res.* **2014**, *53*, 11566–11570. [CrossRef]

32. Yang, Y.; Yin, L.C.; Gong, Y.; Niu, P.; Wang, J.Q.; Gu, L.; Chen, X.; Liu, G.; Wang, L.; Cheng, H.M. An Unusual Strong Visible-Light Absorption Band in Red Anatase TiO_2 Photocatalyst Induced by Atomic Hydrogen-Occupied Oxygen Vacancies. *Adv. Mater.* **2018**, *30*, 1704479. [CrossRef] [PubMed]

33. Kwon, H.; Sung, J.H.; Lee, Y.; Jo, M.-H.; Kim, J.K. Wavelength-dependent visible light response in vertically aligned nanohelical TiO_2-based Schottky diodes. *Appl. Phys. Lett.* **2018**, *112*, 043106. [CrossRef]

34. Flanigan, P.M.; Brady, J.J.; Judge, E.J.; Levis, R.J. Determination of Inorganic Improvised Explosive Device Signatures Using Laser Electrospray Mass Spectrometry Detection with Offline Classification. *Anal. Chem.* **2011**, *83*, 7115–7122. [CrossRef] [PubMed]

35. Wang, D.; Chen, A.; Jang, S.-H.; Yip, H.-L.; Jen, A.K.-Y. Sensitivity of titania(B) nanowires to nitroaromatic and nitroamino explosives at room temperature via surface hydroxyl groups. *J. Mater. Chem.* **2011**, *21*, 7269–7273. [CrossRef]